Neodymium isotopes trace marine provenance of Arctic sea ice

G. Laukert, I. Peeken, D. Bauch, T. Krumpen, E.C. Hathorne, K. Werner, M. Gutjahr, M. Frank

Supplementary Information

The Supplementary Information includes:

- Neodymium Isotope Systematics in the Arctic Ocean
- Sample Collection and Preparation
- Laboratory Analyses
- Back-tracking of Sea Ice Based on Satellite Data
- Tables S-1 to S-8
- Figures S-1 to S-5
- Supplementary Information References

Neodymium Isotope Systematics in the Arctic Ocean

The isotopic composition of neodymium (Nd) is commonly expressed as $\varepsilon_{Nd} = \{(^{143}Nd/^{144}Nd)_{sample}/(^{143}Nd/^{144}Nd)_{CHUR} - 1\} \times 10^4$, with CHUR = 0.512638 (Jacobsen and Wasserburg 1980). In rocks, ε_{Nd} ranges from −56 to +11 on the global scale (Lacan *et al.*, 2012; van de Flierdt *et al.*, 2016). This variability is caused by the fractionation between Nd and samarium (Sm) during magmatic processes and the decay of ^{147}Sm to ^{143}Nd, which together result in more radiogenic (*i.e.* more positive) ε_{Nd} signatures in young mantle-derived rocks compared to old continental rocks. Water masses acquire these distinct rock signatures mainly at the land-ocean interface after their introduction through weathered continental material via rivers, groundwater and coastal erosion. Tracing of the seawater (*i.e.* dissolved) signatures and the water masses they are carried by is enabled by the quasi-conservative behaviour of Nd in the open ocean (Frank, 2002; Goldstein and Hemming, 2003) and its intermediate average oceanic residence time of several hundred years (Tachikawa *et al.*, 2003; Arsouze *et al.*, 2009; Rempfer *et al.*, 2011; Pöppelmeier *et al.*, 2020).

In the Arctic Ocean, seawater ε_{Nd} signatures have been attributed primarily to terrestrial inputs and water mass circulation and mixing, whereas ε_{Nd} changes associated with seawater-particle interactions have been shown to be restricted to certain shelf regions (Andersson *et al.*, 2008; Porcelli *et al.*, 2009; Charette *et al.*, 2016; Laukert *et al.*, 2017a, 2017b, 2017c, 2019; Paffrath *et al.*, 2021a, 2021b). The main Nd sources of the Arctic Ocean and their ε_{Nd} are shown in Fig. S-1. The Atlantic-derived waters dominate the Nd budget with ε_{Nd} signatures around −13 at the Iceland-Scotland Ridge and the Denmark Strait (Laukert *et al.*, 2017a and references therein). Pacific-derived waters entering the Arctic Ocean through the Bering Strait have more radiogenic ε_{Nd} signatures around −3 to −2, which are slightly modified in the Chukchi Sea resulting in ε_{Nd} signatures of −5.5 entering the open Arctic Ocean (Charette *et al.*, 2016).

Freshwater introduced by the various Arctic rivers has a wide range in ε_{Nd} compositions from −17 to −5 (Porcelli *et al.*, 2009; Zimmermann *et al.*, 2009; Persson *et al.*, 2011; Laukert *et al.*, 2017a, 2017b). Significantly less radiogenic signatures (<−17) are only introduced through discharge from Greenland and the Canadian Arctic Archipelago (Filippova *et al.*, 2017; Laukert *et al.*, 2018; Grenier *et al.*, 2022). The sea ice cover prevents aeolian Nd to reach the entire Arctic Ocean in winter and year-round in the central Arctic Ocean. Instead, atmospheric Nd is likely trapped in snow deposited on sea ice and released only during the melt season.

All published ε_{Nd} data for surface seawater are shown in Figure S-1 in addition to major external Nd sources. Despite considerable mixing, laterally and vertically separated contributions from the Lena and Yenisei/Ob rivers were recently identified in the central Arctic Ocean and considered as different source clusters of the Transpolar Drift (Paffrath *et al.*, 2021a). Similar provenance tracer characteristics have been observed in the northern Laptev Sea (Laukert *et al.*, 2017b), suggesting that the Laptev Sea is the main source region for freshwater, nutrients, and trace elements transported via the Transpolar Drift. Depending on the wind fields, the Lena plume is transported either northward or eastward (Janout *et al.*, 2020), resulting in spatiotemporal variability in the distribution of source tracers within the Transpolar Drift.

Sample Collection and Preparation

Sampling of sea ice, snow and seawater was carried out during the PS85 cruise with the RV *Polarstern* in the Fram Strait in June and July 2014. At each ice station, a designated coring site was assigned and, if present, the snow was sampled prior to the drilling of the sea ice cores. Several ice cores free of ice rafted detrital material based on visual inspection were taken at each station, one of which was used for high-resolution temperature and salinity profiles and another one for tracer analysis. Nitrile gloves were used during sampling and cores were drilled with a Kovacs 9 cm diameter corer (Kovacs Enterprise, Roseburg, USA). The temperature of the ice was directly measured on the floe by drilling into the ice and determining the temperature every 5 cm with a Testo 720 RTD thermometer. Thereafter the core was sectioned in 10 cm pieces and weighted to calculate the brine volume. After melting the salinity was determined with a WTW salinity probe. The ice cores were immediately transferred into plastic bags (LDPE tube films by Rische and Herfurth) and stored at −20 °C. Snow was collected with an acid-cleaned plastic shovel and stored at −20 °C in acid-cleaned plastic bags. A SBE32 rosette water sampler equipped with 24 Niskin-type sample bottles (12 L) was used for collection of the seawater samples, which were directly filtered through AcroPakTM500 Capsules with Supor Membrane (pore size, 0.8/0.2µm) filter cartridges, collected in 20 L acid-cleaned LDPE-containers and stored on board.

The frozen sea ice samples were transported to GEOMAR and processed in the clean room laboratory (MK-Versuchsanlagen, class 100 hoods) immediately after removal from the freezer. All mechanical work on the ice cores was carried out on a clean plastic table covered with acid-cleaned Teflon foil. To remove contaminants from the surfaces of the sea ice samples, the ice cores were rinsed with deionised water (18.2 MΩ cm, Milli-Q system) at a temperature of ~20 °C for about 15 seconds. Subsequently, the top surface of the ice cores was scraped off with a custom-made titanium grade 1 chisel. The cores were then split into several pieces with a titanium grade 1 hammer and put into acid-cleaned LDPE-buckets with closed plastic lids for melting. No release of brine water was observed throughout the sample processing period. The ice melted within ~12 h or less, and the meltwater samples were filtered through Merck Millipore® 0.45 µm cellulose acetate filters immediately after the last piece of ice melted. The meltwater was then transferred to acid-cleaned LDPE cubitainers. The snow samples were treated similarly to the sea-ice samples, except that they were not rinsed with deionised water (this was not necessary given that the plastic bags in which the snow was stored were acid-cleaned). After sub-sampling of sea ice and snow meltwater for salinity and stable oxygen isotope analysis as well as REE ultrafiltration, the filtered sea ice, snow and seawater samples were acidified to pH ≈ 2.2 with ultra-pure concentrated hydrochloric acid and at least 48 h for equilibration were given before another aliquot was separated into an acid-cleaned LDPE-bottle for REE concentration and other analyses.

Ultrafiltration of the sea ice and snow meltwater for REE analysis was performed immediately after initial filtration through Merck Millipore 0.45 µm cellulose acetate filters. Amicon® Ultra-15 centrifugal filter units with a volume of 15 mL and either 3000 or 30,000 Nominal Molecular Weight Limit (*i.e.* 3 or 30 kDa) were used. The tubes were first acid-cleaned and deionised water (18.2 MΩ cm, Milli-Q system) was filtered twice before the actual sample was filtered and collected. Filtration was carried out at 3500 rpm for 20 minutes. The samples were then acidified to a pH of ~2.2 with ultra-pure concentrated hydrochloric acid before further processing.

Laboratory Analyses

Radiogenic neodymium isotopes

The entire pre-concentration, purification and measurement techniques reported here strictly followed approved GEOTRACES protocols and were confirmed through participation in the international GEOTRACES inter-calibration study (van de Flierdt *et al.*, 2012). To each seawater, sea ice and snow sample trace metal clean $FeCl_3$ solution was added (~200 mg Fe/mL) and the samples were left for equilibration for 24 h before trace metal clean ammonia solution (25 %, Merck Suprapur®) was added to raise the pH to 7.5–8.0. After 48 h, the co-precipitated trace elements settled to the bottom of the cubitainers together with FeOOH and the supernatant water was syphoned off. The precipitates were centrifuged and rinsed three times with deionised water (MilliQ, 18.2 MΩcm) in 50 mL centrifuge tubes to remove major ions, transferred into 60 mL PFA vials with 6 M HCl and then evaporated to dryness. To remove organic components, the samples were treated with aqua regia at 120 °C for 24 h. After evaporation to dryness, the samples were dissolved in 6 M HCl and the sample in solution was washed with pre-cleaned di-ethyl ether to remove 99 % of the Fe (Stichel *et al.*, 2012), dried down and dissolved in 1 M HCl for column chemistry. The REEs were separated from matrix elements through cation exchange chromatography (BIORAD®, AG50W-X8 resin, 200–400 µm mesh-size, 1.4 mL resin bed) with a slightly modified separation scheme of Stichel *et al.* (2012), where instead of a mixture of HCl and HF acids only HCl was used as a reagent. Nd was further purified from the other REEs for isotope measurements using Eichrom® LN-Spec resin (2 mL, 50–100 µm) following previously established procedures (Pin and Zalduegui, 1997; Le Fèvre and Pin, 2005). To destroy residual traces of the resin and organic compounds the samples were finally treated with concentrated quartz-distilled HNO_3 before Nd isotope measurements.

The $^{143}Nd/^{144}Nd$ ratios were measured on a Neptune Plus MC-ICP-MS (40 cycles at 4 s, 10^{12} Ω resistors assigned to masses 143 and 146) and were double-corrected for instrumental mass bias to $^{146}Nd/^{144}Nd = 0.7219$ and to $^{142}Nd/^{144}Nd = 1.141876$, provided that the ^{142}Ce beam intensity was sufficiently low (Vance and Thirwall, 2002), monitored via ensuring a raw measured $^{140}Ce/^{144}Nd < 1$ (*i.e.* $Ce/Nd < 0.3$) for each sample and standard solution. Isobaric interferences between ^{144}Sm and ^{144}Nd were corrected by measuring the abundance of the interference free isotope ^{147}Sm and by calculating the potential ^{144}Sm contribution on mass 144 from the natural abundance of Sm. The $^{143}Nd/^{144}Nd$ ratios of all samples were normalised to the accepted JNdi-1 standard value of 0.512115 (Tanaka *et al.*, 2000). The external reproducibility of the Nd isotope measurements as estimated by repeated measurements of the JNdi-1 standard at concentrations matched to fit to those of the samples (between 0.2 and 3 ng, $n = 4$) ranged between 0.5 and 3.6 ε_{Nd} units (2 s.d.). Some of the snow and sea ice samples had a low Nd yield likely due to loss during column chemistry. The procedural laboratory blanks ($n = 3$) had <10 pg, which corresponds to <6 % of the lowest Nd concentration used for the isotope measurements. Blank corrections were not applied, and blank contributions are provided in % in Tables S-2 and S-3.

Rare earth element concentrations

The REE concentrations were determined for filtered and ultrafiltered samples using an online pre-concentration (OP) ICP-MS technique at GEOMAR by directly coupling a "seaFAST" system (Elemental Scientific Inc., Nebraska, USA) to an ICP-MS (Agilent 7500ce) (Hathorne *et al.*, 2012). The method of Hathorne *et al.* (2012) was further improved by using an 8 mL sample loop and by preparation of calibration standards with a mixed REE solution of a seawater-like composition in a natural seawater matrix (Osborne *et al.*, 2015). Repeated measurements of GEOTRACES intercalibration sample BATS 2000m (van de Flierdt *et al.*, 2012) and the diluted (500×) reference material SLRS-4 were used to monitor the external reproducibility, which based on BATS 2000m was better than ~6 %, ~7 % and ~11 % for the LREEs, MREEs and HREEs, respectively, and based on SLRS-4 was better than ~8 %, ~18 % and ~34 %, respectively. We diluted SLRS-4 to monitor the accuracy and precision of measurements of snow and sea ice samples with similarly low REE concentrations. The measured REE of SLRS-4 and BATS 2000m agree well with literature values (Table S-8). The procedural laboratory blanks (n = 3, filtered and ultrafiltered) had similar REE concentrations on average corresponding to less than 5 % of sea ice and snow samples analysed, except for Ce which was on average ~7 % (Table S-8).

Stable oxygen isotopes and sample salinity

Oxygen isotope compositions were analysed at the Stable Isotope Laboratory of the College of Earth, Ocean, and Atmospheric Sciences at Oregon State University (Corvallis, USA) applying a CO_2-water isotope equilibration technique (Epstein and Mayeda, 1953) on at least two subsamples on a DeltaPlusXL instrument. The external reproducibility for the $\delta^{18}O$ measurements was ±0.04 ‰ or better and the measured $^{18}O/^{16}O$ ratio is provided as a deviation from Vienna Standard Mean Ocean Water in the δ-notation (Craig, 1961). Sample salinity was determined with an AutoSal 8400A salinometer at GEOMAR with a precision of ±0.003 and an accuracy better than ±0.005.

Back-tracking of Sea Ice Based on Satellite Data

Pathways, age and source area of sampled sea ice were investigated with the AWI IceTrack system (Krumpen *et al.*, 2020). The low-resolution sea ice drift product OSI-405-c from the Ocean and Sea Ice Satellite Application Facility (OSI SAF; Lavergne, 2016; 62.5 × 62.5 km grid spacing) is used to trace sea ice backward in time until sea-ice concentration at a specific location drops below a predefined threshold (here 50 %) and we assume the ice to be formed. The sea-ice concentration product is based on the 85 GHz Special Sensor Microwave/Imager (SSM/I) and provided by CERSAT (Ezraty *et al.*, 2007; 12.5 km resolution). To assess the accuracy of this Lagrangian tracking approach, Krumpen *et al.* (2019) reconstructed the pathways of 56 GPS buoys deployed between 2011 and 2016 in the central Arctic Ocean. The displacement between real and virtual tracks is rather small (36 ± 20 km after 200 days). However, the accuracy of the method is lower in Fram Strait, likely due to a general underestimation of drift velocities by low-resolution satellite products in this area (Krumpen *et al.*, 2021) (Fig. 2c). Therefore, in this study, the sampled sea ice in Fram Strait was first manually tracked for a short distance using optical satellite data (MODIS - provided via https://worldview.earthdata.nasa.gov) before tracking was continued with IceTrack.

Supplementary Tables

Table S-1 Sea ice and snow sampling and accompanying information.

Table S-2 Salinity, $\delta^{18}O$ and dissolved (<0.45 μm) ε_{Nd} compositions of sea ice.

Table S-3 Salinity, $\delta^{18}O$ and dissolved (<0.45 μm) ε_{Nd} compositions of snow.

Table S-4 Dissolved (<0.45 μm) and truly dissolved (<30 kDa and 3 kDa) REE concentrations of sea ice.

Table S-5 Dissolved (<0.45 μm) and truly dissolved (<30 kDa and 3 kDa) REE concentrations of snow.

Table S-6 Dissolved (<0.2 μm) ε_{Nd} compositions and REE concentrations of surface seawater.

Table S-7 High-resolution temperature and salinity profiles of sea ice cores from same stations.

Table S-8 REE concentrations of reference materials SLRS-4 (500× dilution), BATS 2000m and blanks.

Tables S-1 to S-8 are available for download (Excel) from the online version of the article at https://doi.org/10.7185/geochemlet.2220.

Supplementary Figures

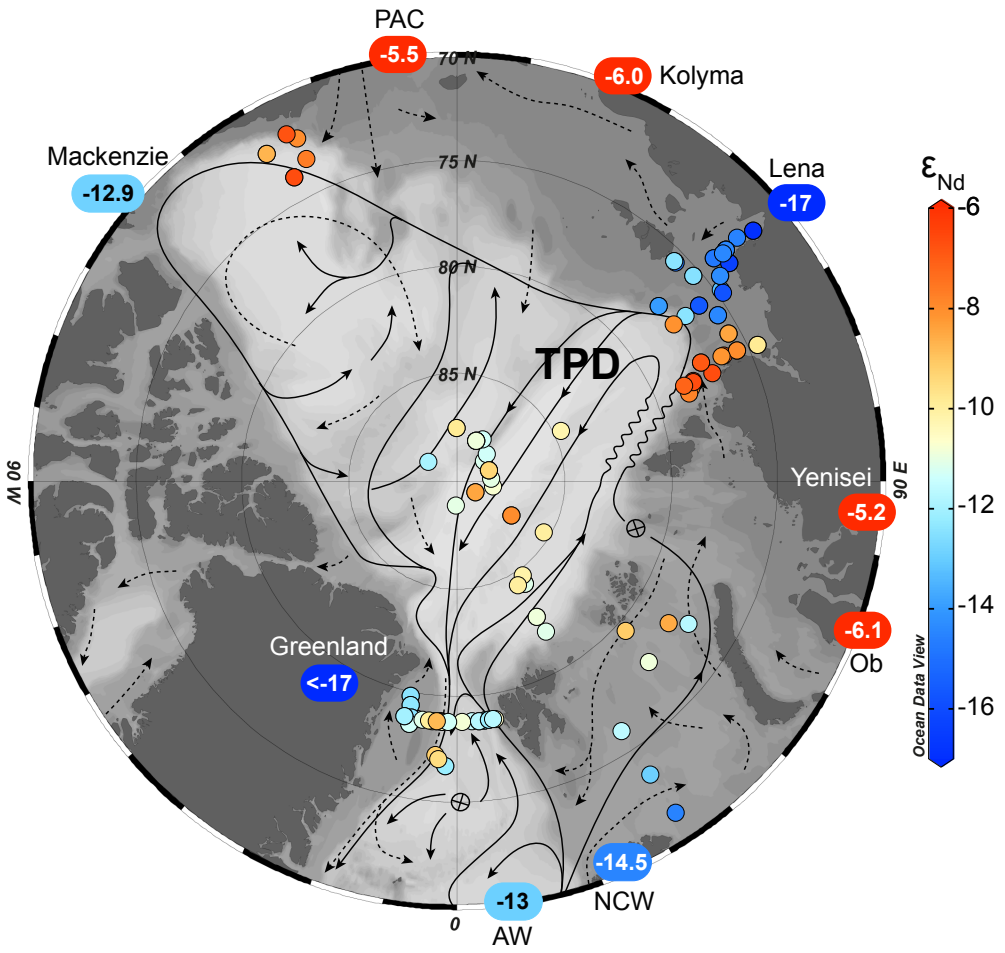

Figure S-1 Bathymetric map of the Arctic Ocean (IBCAO; Jakobsson *et al.*, 2012) with major Nd sources and their ε_{Nd} signatures as well as published surface seawater ε_{Nd} data (Andersson *et al.*, 2008; Porcelli *et al.*, 2009; Zimmermann *et al.*, 2009; Persson *et al.*, 2011; Charette *et al.*, 2016; Laukert *et al.*, 2017a, 2017b; Paffrath *et al.*, 2021a). The Transpolar Drift (TPD) and the general circulation pattern of surface (dashed black arrows) and AW (black arrows) waters are shown in addition (modified after Rudels *et al.*, 2012). The known Nd sources are Atlantic-derived waters (AW) entering through the Iceland-Scotland Ridge and the Denmark Strait, Norwegian Coastal Water (NCW), modified Pacific-derived waters (PAC), major Siberian Rivers (Ob, Yenisei, Lena, Kolyma), and the Mackenzie River.

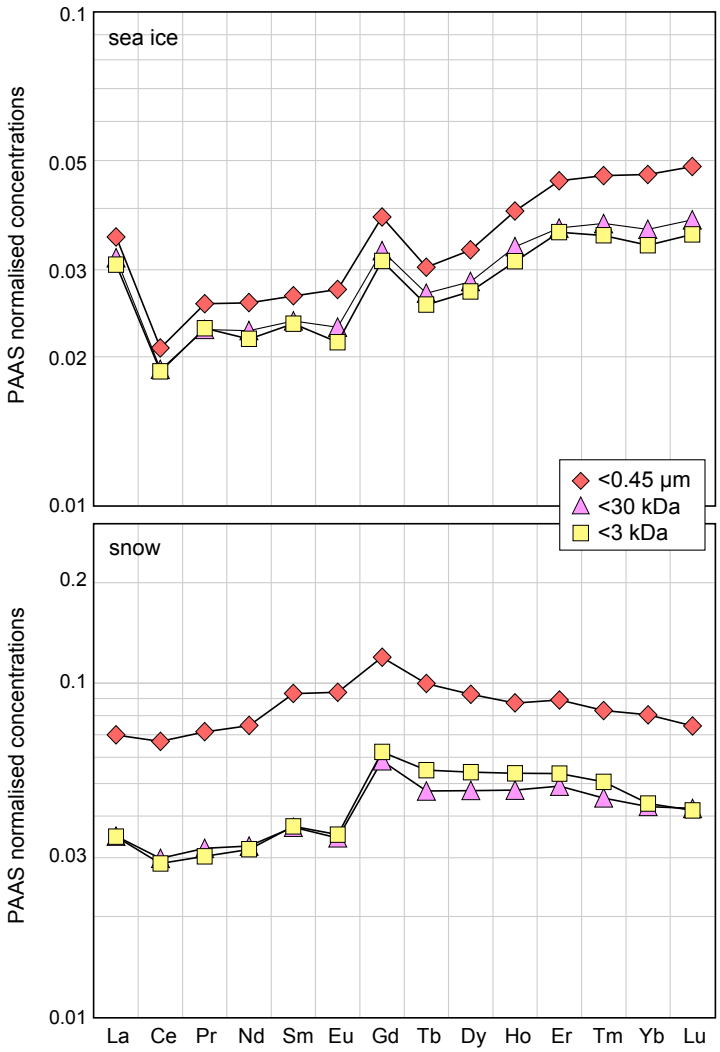

Figure S-2 Averaged rare earth element (REE) concentrations of the different size pools in sea ice (upper figure) and snow (lower figure) samples normalised to Post Archaean Australian Shale ($\times 10^6$; McLennan, 2001).

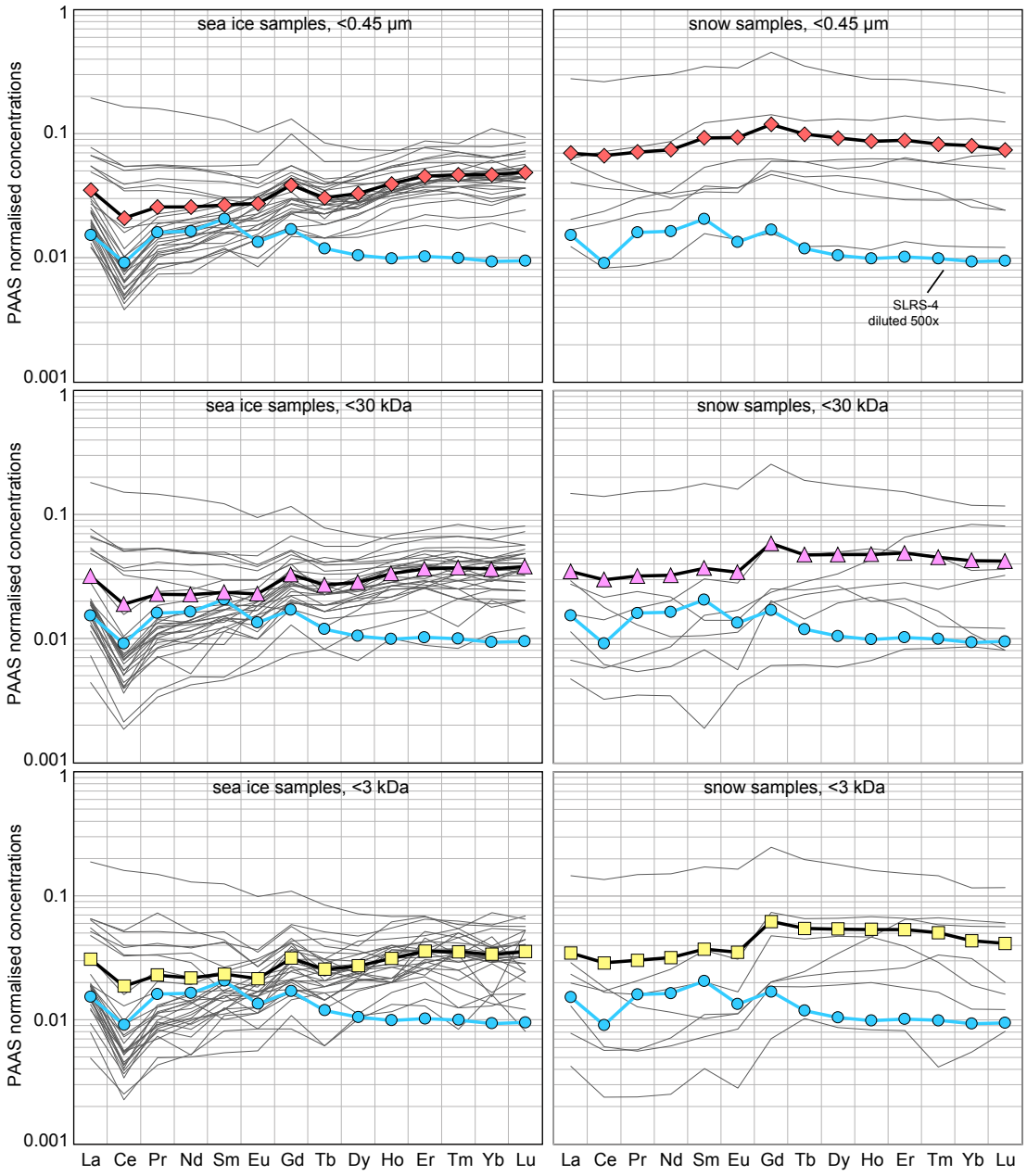

Figure S-3 Rare earth element (REE) concentrations of all sea ice and snow samples normalised to Post Archaean Australian Shale ($\times 10^6$; McLennan, 2001) with the corresponding averages (same colours as in Fig. S-1). For comparison, the reference material SLRS-4 is shown (500× dilution).

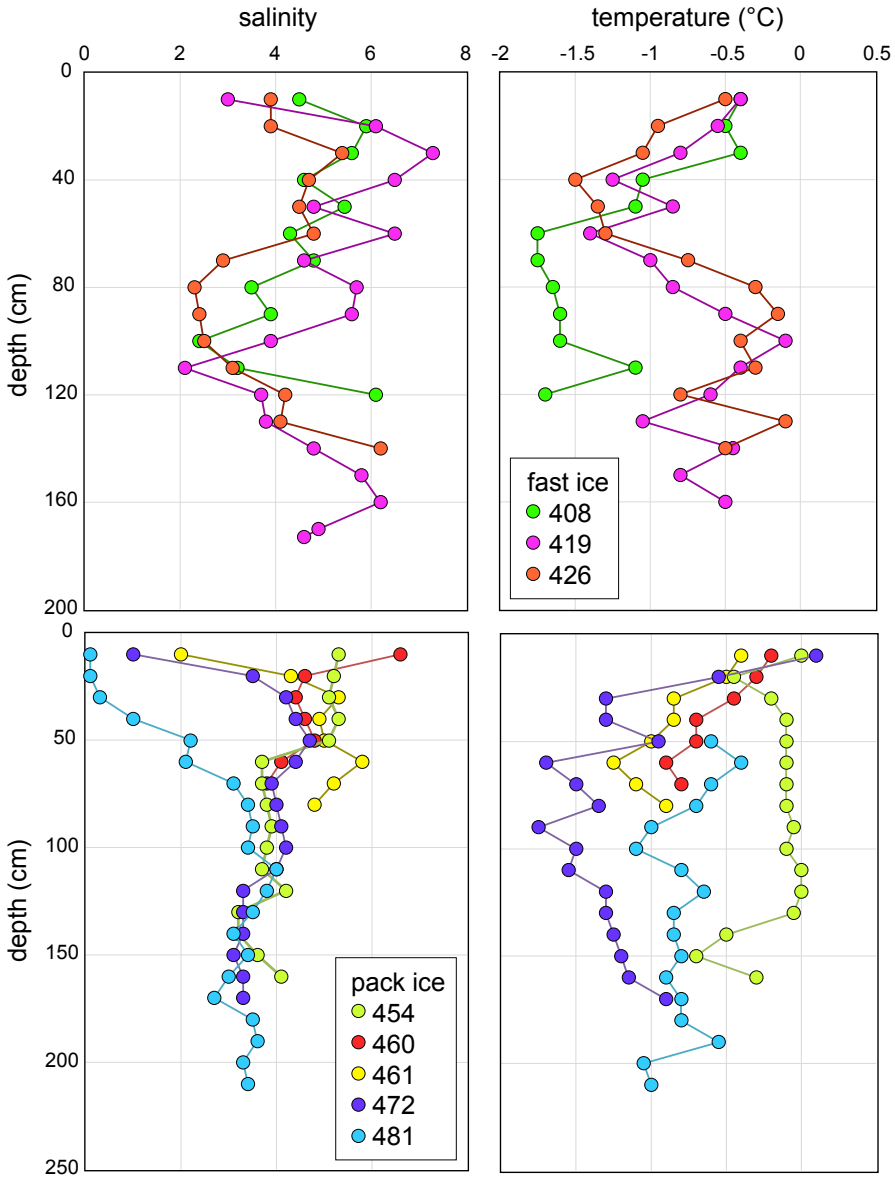

Figure S-4 High-resolution temperature and salinity profiles of fast ice (upper figures) and pack ice (lower figures). Temperature was averaged from 5 cm intervals.

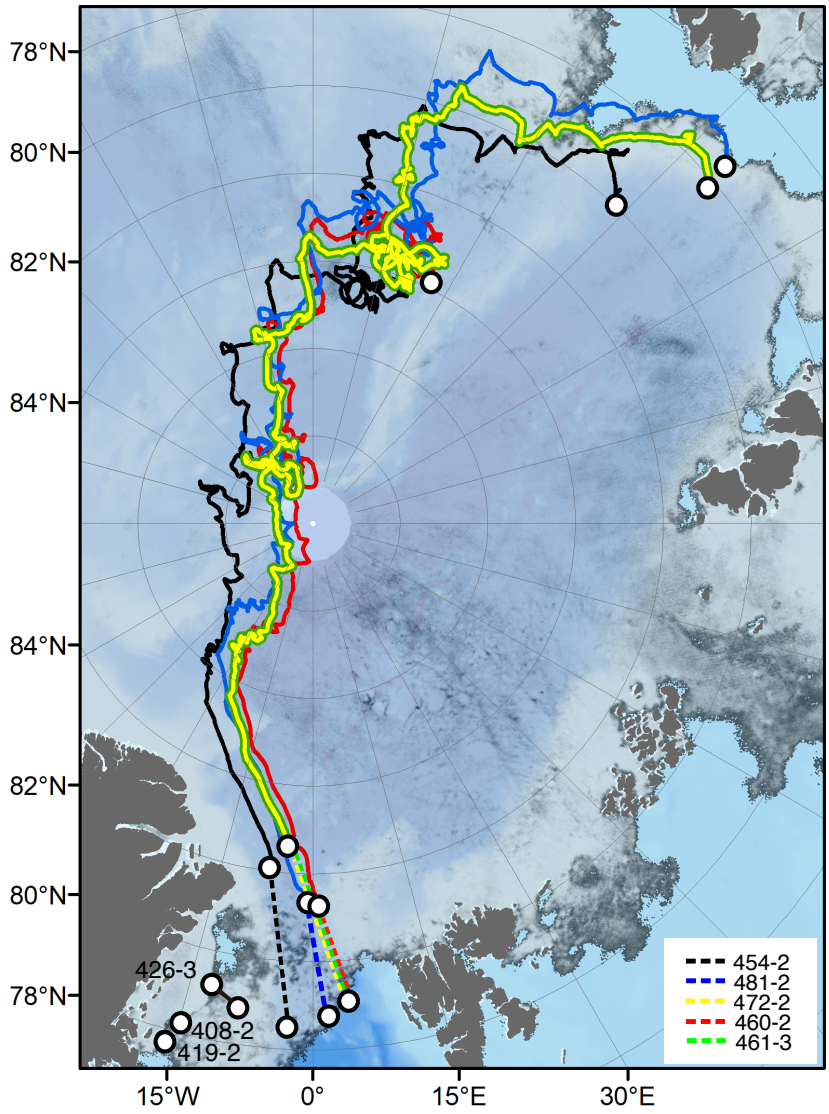

Figure S-5 Reconstructed sea ice origin and drift trajectories from short-distance manual tracking (all fast ice stations and dashed lines for pack ice) using optical satellite data (MODIS - provided via https://worldview.earthdata.nasa.gov) and long-distance tracking (solid lines, only pack ice) based on the AWI IceTrack system (Krumpen *et al.*, 2020).

Supplementary Information References

Andersson, P.S., Porcelli, D., Frank, M., Bjork, G., Dahlqvist, R., Gustafsson, O. (2008) Neodymium isotopes in seawater from the Barents Sea and Fram Strait Arctic-Atlantic gateways. *Geochimica et Cosmochimica Acta* 72, 2854–2867. https://doi.org/10.1016/j.gca.2008.04.008

Arsouze, T., Dutay, J.-C., Lacan, F., Jeandel, C. (2009) Reconstructing the Nd oceanic cycle using a coupled dynamical – biogeochemical model. *Biogeosciences* 6, 2829–2846. https://doi.org/10.5194/bg-6-2829-2009

Charette, M.A., Lam, P.J., Lohan, M.C., Kwon, E.Y., Hatje, V., *et al*. (2016) Coastal ocean and shelf-sea biogeochemical cycling of trace elements and isotopes: lessons learned from GEOTRACES. *Philosophical Transactions of the Royal Society A: Mathematical, Physical and Engineering Sciences* 374, 20160076. https://doi.org/10.1098/rsta.2016.0076

Craig, H. (1961) Isotopic Variations in Meteoric Waters. *Science* 133, 1702–1703. https://doi.org/10.1126/science.133.3465.1702

Epstein, S., Mayeda, T. (1953) Variation of O^{18} content of waters from natural sources. *Geochimica et Cosmochimica Acta* 4, 213–224. https://doi.org/10.1016/0016-7037(53)90051-9

Ezraty, R., Girard-Ardhuin, F., Piolle, J.F., Kaleschke, L., Heygster, G. (2007) *Arctic and Antarctic Sea Ice Concentration and Arctic Sea Ice Drift Estimated from Special Sensor Microwave Data – User's manual V2.1*. Technical Report, Département d'Océanographie Physique et Spatiale, IFREMER, Brest, France.

Filippova, A., Frank, M., Kienast, M., Rickli, J., Hathorne, E.C., Yashayaev, I.M., Pahnke, K. (2017) Water mass circulation and weathering inputs in the Labrador Sea based on coupled Hf–Nd isotope compositions and rare earth element distributions. *Geochimica et Cosmochimica Acta* 199, 164–184. https://doi.org/10.1016/j.gca.2016.11.024

Frank, M. (2002) Radiogenic isotopes: tracers of past ocean circulation and erosional input. *Reviews of Geophysics* 40, 1–38. https://doi.org/10.1029/2000RG000094

Goldstein, S.L., Hemming, S.R. (2003) 6.17 - Long-lived Isotopic Tracers in Oceanography, Paleoceanography, and Ice-sheet Dynamics. In: Holland, H.D., Turekian, K.K. (Eds.) *Treatise on Geochemistry, Volume 6: The Oceans and Marine Geochemistry*. First Edition, Elsevier, Amsterdam, 453–489. https://doi.org/10.1016/B0-08-043751-6/06179-X

Grenier, M., Brown, K.A., Colombo, M., Belhadj, M., Baconnais, I., Pham, V., Soon, M., Myers, P.G., Jeandel, C., François, R. (2022) Controlling factors and impacts of river-borne neodymium isotope signatures and rare earth element concentrations supplied to the Canadian Arctic Archipelago. *Earth and Planetary Science Letters* 578, 117341. https://doi.org/10.1016/j.epsl.2021.117341

Hathorne, E.C., Haley, B.A., Stichel, T., Grasse, P., Zieringer, M., Frank, M. (2012) Online preconcentration ICP-MS analysis of rare earth elements in seawater. *Geochemistry, Geophysics, Geosystems* 13, Q01020. https://doi.org/10.1029/2011GC003907

Jacobsen, S.B., Wasserburg, G.J. (1980) Sm-Nd Isotopic Evolution of Chondrites. *Earth and Planetary Science Letters* 50, 139–155. https://doi.org/10.1016/0012-821X(80)90125-9

Jakobsson, M., Mayer, L., Coakley, B., Dowdeswell, J.A., Forbes, S., *et al*. (2012) The International Bathymetric Chart of the Arctic Ocean (IBCAO) Version 3.0. *Geophysical Research Letters* 39, L12609. https://doi.org/10.1029/2012GL052219

Janout, M.A., Hölemann, J., Laukert, G., Smirnov, A., Krumpen, T., Bauch, D., Timokhov, L. (2020) On the Variability of Stratification in the Freshwater-Influenced Laptev Sea Region. *Frontiers in Marine Science* 7, 543489. https://doi.org/10.3389/fmars.2020.543489

Krumpen, T., Belter, H.J., Boetius, A., Damm, E., Haas, C., Hendricks, S., Nicolaus, M., Nöthig, E.-M., Paul, S., Peeken, I., Ricker, R., Stein, R. (2019) Arctic warming interrupts the Transpolar Drift and affects long-range transport of sea ice and ice-rafted matter. *Scientific Reports* 9, 1–9. https://doi.org/10.1038/s41598-019-41456-y

Krumpen, T., Birrien, F., Kauker, F., Rackow, T., von Albedyll, L., *et al*. (2020) The MOSAiC ice floe: sediment-laden survivor from the Siberian shelf. *The Cryosphere* 14, 2173–2187. https://doi.org/10.5194/tc-14-2173-2020

Krumpen, T., von Albedyll, L., Goessling, H.F., Hendricks, S., Juhls, B., Spreen, G., Willmes, S., Belter, H.J., Dethloff, K., Haas, C., Kaleschke, L., Katlein, C., Tian-Kunze, X., Ricker, R., Rostosky, P., Rückert, J., Singha, S., Sokolova, J. (2021) MOSAiC drift expedition from October 2019 to July 2020: sea ice conditions from space and comparison with previous years. *The Cryosphere* 15, 3897–3920. https://doi.org/10.5194/tc-15-3897-2021

Lacan, F., Tachikawa, K., Jeandel, C. (2012) Neodymium isotopic composition of the oceans: A compilation of seawater data. *Chemical Geology* 300–301, 177–184. https://doi.org/10.1016/j.chemgeo.2012.01.019

Lavergne, T. (2016) *Validation and Monitoring of the OSI SAF Low Resolution Sea Ice Drift Product (v5)*. The EUMETSAT Network of Satellite Application Facilities, Technical Report SAF/OSI/CDOP/Met.no/T&V/RP/131. https://doi.org/10.13140/RG.2.1.4155.5449

Laukert, G., Frank, M., Bauch, D., Hathorne, E.C., Rabe, B., von Appen, W.-J., Wegner, C., Zieringer, M., Kassens, H. (2017a) Ocean circulation and freshwater pathways in the Arctic Mediterranean based on a combined Nd isotope, REE and oxygen isotope section across Fram Strait. *Geochimica et Cosmochimica Acta* 202, 285–309. https://doi.org/10.1016/j.gca.2016.12.028

Laukert, G., Frank, M., Bauch, D., Hathorne, E.C., Gutjahr, M., Janout, M., Hölemann, J. (2017b) Transport and transformation of riverine neodymium isotope and rare earth element signatures in high latitude estuaries: a case study from the Laptev Sea. *Earth and Planetary Science Letters* 477, 205–217. https://doi.org/10.1016/j.epsl.2017.08.010

Laukert, G., Frank, M., Hathorne, E.C., Krumpen, T., Rabe, B., Bauch, D., Werner, K., Peeken, I., Kassens, K. (2017c) Pathways of Siberian freshwater and sea ice in the Arctic Ocean traced with radiogenic neodymium isotopes and rare earth elements. *Polarforschung* 87, 3–13. https://doi.org/10.2312/polarforschung.87.1.3

Laukert, G., Dreyer, J., Frank, M., Hathorne, E.C., Meulenbroek, K. (2018) Greenland-sourced freshwater traced by radiogenic neodymium isotopes and rare earth elements on the North-East Greenland Shelf. *Goldschmidt Abstracts* 2018, 1419. https://goldschmidtabstracts.info/2018/1419.pdf

Laukert, G., Makhotin, M., Petrova, M.V., Frank, M., Hathorne, E.C., Bauch, D., Böning, P., Kassens, H. (2019) Water mass transformation in the Barents Sea inferred from radiogenic neodymium isotopes, rare earth elements and stable oxygen isotopes. *Chemical Geology* 511, 416–430. https://doi.org/10.1016/j.chemgeo.2018.10.002

Le Fèvre, B., Pin, C. (2005) A straightforward separation scheme for concomitant Lu–Hf and Sm–Nd isotope ratio and isotope dilution analysis. *Analytica Chimica Acta* 543, 209–221. https://doi.org/10.1016/j.aca.2005.04.044

McLennan, S.M. (2001) Relationships between the trace element composition of sedimentary rocks and upper continental crust. *Geochemistry, Geophysics, Geosystems* 2, 2000GC000109. https://doi.org/10.1029/2000GC000109

Osborne, A.H., Haley, B.A., Hathorne, E.C., Plancherel, Y., Frank, M. (2015) Rare earth element distribution in Caribbean seawater: Continental inputs versus lateral transport of distinct REE compositions in subsurface water masses. *Marine Chemistry* 177, 172–183. https://doi.org/10.1016/j.marchem.2015.03.013

Paffrath, R., Laukert, G., Bauch, D., Rutgers van der Loeff, M., Pahnke, K. (2021a) Separating individual contributions of major Siberian rivers in the Transpolar Drift of the Arctic Ocean. *Scientific Reports* 11, 8216. https://doi.org/10.1038/s41598-021-86948-y

Paffrath, R., Pahnke, K., Böning, P., Rutgers van der Loeff, M., Valk, O., Gdaniec, S., Planquette, H. (2021b) Seawater-particle interactions of rare earth elements and neodymium isotopes in the deep central Arctic Ocean. *Journal of Geophysical Research: Oceans* 126, e2021JC017423. https://doi.org/10.1029/2021JC017423

Persson, P.O., Andersson, P.S., Porcelli, D., Semiletov, I. (2011) The influence of Lena River water inflow and shelf sediment-sea water exchange for the Nd isotopic composition in the Laptev Sea and Arctic Ocean. *EGU General Assembly Conference Abstracts* 13, EGU2011-672.

Pin, C., Zalduegui, J.F.S. (1997) Sequential separation of light rare-earth elements, thorium and uranium by miniaturized extraction chromatography: Application to isotopic analyses of silicate rocks. *Analytica Chimica Acta* 339, 79–89. https://doi.org/10.1016/S0003-2670(96)00499-0

Porcelli, D., Andersson, P.S., Baskaran, M., Frank, M., Bjork, G., Semiletov, I. (2009) The distribution of neodymium isotopes in Arctic Ocean basins. *Geochimica et Cosmochimica Acta* 73, 2645–2659. https://doi.org/10.1016/j.gca.2008.11.046

Pöppelmeier, F., Scheen, J., Blaser, P., Lippold, J., Gutjahr, M., Stocker, T.F. (2020) Influence of Elevated Nd Fluxes on the Northern Nd Isotope End Member of the Atlantic During the Early Holocene. *Paleoceanography and Paleoclimatology*, 35, e2020PA003973. https://doi.org/10.1029/2020PA003973

Rempfer, J., Stocker, T.F., Joos, F., Dutay, J.C., Siddall, M. (2011) Modelling Nd-isotopes with a coarse resolution ocean circulation model: Sensitivities to model parameters and source/sink distributions. *Geochimica et Cosmochimica Acta* 75, 5927–5950. https://doi.org/10.1016/j.gca.2011.07.044

Rudels, B., Anderson, L., Eriksson, P., Fahrbach, E., Jakobsson, M., Jones, E.P., Melling, H., Prinsenberg, S., Schauer, U., Yao, T. (2012) Observations in the Ocean. In: Lemke, P., Jacobi, H.W. (Eds.) *Atmospheric and Oceanographic Sciences Library, Volume 43: Arctic Climate Change*. Springer Dordrecht, 117–198. https://doi.org/10.1007/978-94-007-2027-5_4

Stichel, T., Frank, M., Rickli, J., Haley, B.A. (2012) The hafnium and neodymium isotope composition of seawater in the Atlantic sector of the Southern Ocean. *Earth and Planetary Science Letters* 317–318, 282–294. https://doi.org/10.1016/j.epsl.2011.11.025
Tachikawa, K., Athias, V., Jeandel, C. (2003) Neodymium budget in the modern ocean and paleo-oceanographic implications. *Journal of Geophysical Research: Oceans* 108, 3254. https://doi.org/10.1029/1999JC000285

Tanaka, T., Togashi, S., Kamioka, H., Amakawa, H., Kagami, H., Hamamoto, T., Yuhara, M., Orihashi, Y., Yoneda, S., Shimizu, H., Kunimaru, T., Takahashi, K., Yanagi, T., Nakano, T., Fujimaki, H., Shinjo, R., Asahara, Y., Tanimizu, M., Dragusanu, C. (2000) JNdi-1: a neodymium isotopic reference in consistency with LaJolla neodymium. *Chemical Geology* 168, 279–281. https://doi.org/10.1016/S0009-2541(00)00198-4

van de Flierdt, T., Pahnke, K., Amakawa, H., Andersson, P.S., Basak, C., *et al*. (2012) GEOTRACES intercalibration of neodymium isotopes and rare earth element concentrations in seawater and suspended particles. Part 1: reproducibility of results for the international intercomparison. *Limnology and Oceanography: Methods* 10, 234–251. https://doi.org/10.4319/lom.2012.10.234

van de Flierdt, T., Griffiths, A.M., Lambelet, M., Little, S.H., Stichel, T., Wilson, D.J. (2016) Neodymium in the oceans: a global database, a regional comparison and implications for palaeoceanographic research. *Philosophical Transactions of the Royal Society A: Mathematical, Physical and Engineering Sciences* 374, 20150293. https://doi.org/10.1098/rsta.2015.0293

Vance, D., Thirlwall, M. (2002) An assessment of mass discrimination in MC-ICPMS using Nd isotopes. *Chemical Geology* 185, 227–240. https://doi.org/10.1016/S0009-2541(01)00402-8

Yeghicheyan, D., Carignan, J., Valladon, M., Bouhnik Le Coz, M., Le Cornec, F., *et al*. (2001) A Compilation of Silicon and Thirty One Trace Elements Measured in the Natural River Water Reference Material SLRS-4 (NRC-CNRC). *Geostandards Newsletter* 25, 465–474. https://doi.org/10.1111/j.1751-908X.2001.tb00617.x

Zimmermann, B., Porcelli, D., Frank, M., Andersson, P.S., Baskaran, M., Lee, D.C., Halliday, A.N. (2009) Hafnium isotopes in Arctic Ocean water. *Geochimica et Cosmochimica Acta* 73, 3218–3233. https://doi.org/10.1016/j.gca.2009.02.028